Video Article

Agarose-based Tissue Mimicking Optical Phantoms for Diffuse Reflectance Spectroscopy

Afrina Mustari*[1], Izumi Nishidate*[1], Md. Abdul Wares[1,6], Takaaki Maeda[2], Satoko Kawauchi[3], Shunichi Sato[3], Manabu Sato[4], Yoshihisa Aizu[5]

[1]Graduate School of Bio-application & Systems Engineering, Tokyo University of Agriculture & Technology

[2]Department of Mechanical Engineering, Kushiro National College of Technology

[3]Division of Bioinformation and Therapeutic Systems, National Defense Medical College Research Institute

[4]Graduate School of Science and Engineering, Yamagata University

[5]College of Design and Manufacturing Technology, Muroran Institute of Technology

[6]Department of Livestock Services, Ministry of Fisheries and Livestock, Government of Bangladesh

*These authors contributed equally

Correspondence to: Izumi Nishidate at inishi@cc.tuat.ac.jp

URL: https://www.jove.com/video/57578
DOI: doi:10.3791/57578

Keywords: Bioengineering, Issue 138, Optical phantom, agarose gel, lipid emulsion, optical properties, hemoglobin, light scattering, light absorption, inverse Monte Carlo simulation, diffuse reflectance spectroscopy

Date Published: 8/22/2018

Citation: Mustari, A., Nishidate, I., Wares, M.A., Maeda, T., Kawauchi, S., Sato, S., Sato, M., Aizu, Y. Agarose-based Tissue Mimicking Optical Phantoms for Diffuse Reflectance Spectroscopy. *J. Vis. Exp.* (138), e57578, doi:10.3791/57578 (2018).

Abstract

This protocol describes how to make agarose-based tissue-mimicking phantoms and demonstrates how to determine their optical properties using a conventional optical system with an integrating sphere. Measuring systems for the acquisition of the diffuse reflectance and total transmittance spectra are constructed with a broadband white light source, a light guide, an achromatic lens, an integrating sphere, a sample holder, an optical fiber probe, and a multi-channel spectrometer. An acrylic mold consisting of two rectangular acrylic pieces and a U-shaped acrylic piece is constructed to create an epidermal phantom and a dermal phantom with whole blood. The application of a sodium dithionite ($Na_2S_2O_4$) solution to the dermal phantom enables the researcher to deoxygenate hemoglobin in red blood cells distributed in the dermal phantom. The inverse Monte Carlo simulation with the diffuse reflectance and total transmittance spectra measured by a spectrometer with an integrating sphere is performed to determine the absorption coefficient spectrum $\mu_a(\lambda)$ and the reduced scattering coefficient spectrum $\mu_s'(\lambda)$ of each layer phantom. A two-layered phantom mimicking the diffuse reflectance of human skin tissue is also demonstrated by piling up the epidermal phantom on the dermal phantom.

Video Link

The video component of this article can be found at https://www.jove.com/video/57578/

Introduction

Optical phantoms are objects mimicking the optical properties of biological tissues and have been widely used in the biomedical optics field. They are designed so that the optical properties, such as light scattering and absorption coefficients, match with those of living human and animal tissues. Optical phantoms are generally used for the following purposes: simulating the light transport in biological tissues, calibrating a newly developed optical system design, evaluating the quality and performance of existing systems, comparing the performance between systems, and validating the ability of the optical methods to quantify the optical properties[1,2,3,4,5]. Therefore, easy-to-get substances, a simple fabrication process, a high reproducibility, and an optical stability are required for making optical phantoms.

Various types of optical phantoms with different base materials such as aqueous suspension[6], gelatin gel[7], agarose gel[8,9,10], polyacrylamide gel[11], resin[12,13,14,15,16], and room-temperature-vulcanizing silicone[17] have been reported in previous literature. It has been reported that gelatin- and alginate-based gels are useful for optical phantoms with heterogeneous structures[18]. Alginate phantoms have a suitable mechanical and thermal stability for evaluating photothermal effects such as laser ablation studies and laser-based hyperthermia studies[18]. Agarose gels have the ability to fabricate heterogeneous structures, and their mechanical and physical properties are stable for a long time[18]. High-purity agarose gels have a very low turbidity and a weak optical absorption. Therefore, optical properties of agarose-based phantoms could easily be designed with the appropriate light scattering and absorbing agents. Recently, styrene-ethylene-butylene-styrene (SEBS) block copolymers[19] and polyvinyl chloride (PVC) gels[20] have been reported as interesting phantom materials for optical and photoacoustic techniques.

Polymer microspheres[7,12,21,22], titanium oxide powder[1], and lipid emulsions[23,24,25,26] such as milk and lipid emulsion are used as light scattering agents, whereas black ink[27,28] and molecular dyes[29,30] are used as light absorbers. Diffuse reflectance spectra of most living organs are dominated by the absorption of oxygenated and deoxygenated hemoglobin in red blood cells. Therefore, hemoglobin solutions[31,32] and whole blood[8,9,10,33,36] are often used as light absorbers in the phantoms for a diffuse reflectance spectroscopy and multispectral imaging.

The method described in this article is used to create an optical phantom mimicking the light transport in biological tissues and to characterize its optical properties. As an example, a two-layered optical phantom mimicking optical properties of human skin tissue is demonstrated. The advantages of this method over alternative techniques are the ability to represent diffuse reflectance spectra of living biological tissues in the visible to near-infrared wavelength region, as well as the simplicity to make it, using easily available materials and conventional optical instruments. Therefore, the optical phantoms made by this method will be useful for the development of optical methods based on diffuse reflectance spectroscopy and multispectral imaging.

Protocol

1. Construction of a Conventional Diffuse Reflectance and Total Transmittance Spectroscopic System

Note: Construct the measuring systems for the diffuse reflectance and total transmittance spectra using a broadband white light source, a light guide, an achromatic lens, an integrating sphere, a sample holder, an optical fiber, and a multi-channel spectrometer. The role of the light trap is to remove the specular reflection component from the reflectance spectrum. The sample holder of the integrating sphere consists of a mounting plate and a dovetail and spring-loaded clamp assembly that holds the sample against the port. The dovetail and spring-loaded clamp assembly are removed from the sample holder and a hand-made cubic pedestal of polystyrene foam is attached to the mounting plate instead. The layouts of the optical components, shown in **Figure 1a** and **1b**, can be referred to for the construction procedure for the diffuse reflectance measurements and the total transmittance measurements, respectively.

1. Connect the spectrometer and a personal computer using the universal serial bus (USB) cable provided.
2. Attach the port adapter to a detector port of the integrating sphere. Connect the spectrometer and the port adapter of the integrating sphere using an optical fiber. Connect the 150 W halogen lamp light source and the light guide.
3. Attach the sample holder to a sample port of the integrating sphere. Attach the light trap to an appropriate port of the integrating sphere when performing the diffuse reflectance measurements. Turn on the halogen lamp light source to illuminate a sample *via* the light guide and the achromatic lens.
4. Open the operating software of the spectrometer.

2. Preparation of an Acrylic Mold

Note: An acrylic mold that consists of two rectangular acrylic pieces and a U-shaped acrylic piece is constructed to create a monolayer gel phantom. **Figure 2** can be referred to for this construction procedure.

1. Cut out the two rectangular acrylic pieces from a 2-mm-thick acrylic plate to an optional size.
2. Cut out an acrylic piece from a 1-mm-thick acrylic plate to an optional size. Cut the 1-mm-thick acrylic piece so that it becomes a U-shaped piece to be used for the mold to make 1-mm thick epidermal phantoms.
3. Cut out an acrylic piece from a 5-mm-thick acrylic plate to an optional size. Cut the 5-mm-thick acrylic piece so that it becomes a U-shaped piece to be used as a mold to make 5-mm thick dermal phantoms.
4. Remove any burrs from each acrylic piece using a metal file.
5. Make the epidermal phantom mold by holding the 1-mm-thick U-shaped piece with the two 2-mm-thick acrylic pieces and fixing them with five foldback clips.
6. Make the dermal phantom mold by holding the 5-mm-thick U-shaped piece with the two 2-mm-thick acrylic pieces and fixing them with five foldback clips.

3. Preparation of Base Material

1. Put 500 mL of standard saline with 0.9% (w/v) NaCl in a pod. Slowly add 5 g of agarose powder while stirring the mixture to avoid clumping.
2. Heat the mixture of agarose powder and saline by an electric cooking heater with a 1,000 W power setting for 5 min.
3. Once the mixture boils, keep the mixture on low heat for 3 min.
4. Cool the mixture to a temperature of about 70 °C. Then pour the mixture into a container and keep it in a constant temperature bath at 60 °C for 30 min before making a phantom.

4. Preparation of Skin-mimicking Optical Phantoms

Note: A coffee solution is used to mimic the absorption spectrum of melanin. The coffee solution contains a brown pigment called melanoidin. The absorption spectrum of melanoidin has been reported to be similar to that of melanin[10].

1. **Prepare an epidermal phantom**
    1. Pour 100 mL of pure water into the coffee maker reservoir. Place a filter in the coffee maker basket. Add 24 g of ground coffee into the filter. Turn on the coffee maker and press the brew button to begin brewing.
    2. Put 4 mL of brewed coffee and 16 mL of saline in a glass bottle to make a coffee solution.
    3. Put 5 mL of lipid emulsion (*e.g.*, intralipid 10%) and 10 mL of the coffee solution into a transparent plastic cup. Slowly add 35 mL of the base material to this mixture while stirring.
    4. Aspirate the mixture into a syringe and inject it slowly into the epidermal phantom mold while avoiding any bubble formation. Cool the acrylic mold containing the mixture at 5 °C for 20 min.

5. Remove the foldback clips from the mold. Slide one of the acrylic pieces outward and remove it from the mold. Take the 1-mm-thick solidified gel phantom out of the mold and cut it to the desired size using a surgical scalpel.
6. Place and hold the gel phantom between two slide glasses.

2. **Prepare a dermal phantom containing oxygenated blood**
   1. Take 5.0 mL of lipid emulsion and 0.4 mL of whole equine blood with 45%-hematocrit and put into a transparent plastic cup. Slowly add 44.6 mL of the base material while stirring the mixture.
   2. Aspirate the mixture into a syringe and inject it slowly into the dermal phantom mold while avoiding any bubble formation. Cool the acrylic mold containing the mixture at 5 °C for 20 min.
   3. Remove the foldback clips from the mold. Slide one of the acrylic pieces outward and remove it from the mold. Take the 5-mm-thick solidified gel phantom out of the mold and cut it to the desired size using a surgical scalpel.
   4. Place and hold the gel phantom between two slide glasses.

3. **Prepare a dermal phantom containing deoxygenated blood**
   1. Put a dermal gel phantom containing oxygenated blood (from step 4.2.3) on a glass dish.
   2. Dissolve 1 g of sodium dithionite ($Na_2S_2O_4$) into 20 mL of saline in a glass bottle.
   3. Add 0.05 g/mL of $Na_2S_2O_4$ solution onto the phantom using a syringe to deoxygenate the blood in the phantom.
   4. Place and hold the phantom between two slide glasses to prevent it drying out.

4. **Prepare a two-layered phantom**
   1. Drop 0.1 mL of saline onto a dermal phantom to ensure optical coupling between the epidermal and dermal layers. Place the epidermal phantom on the dermal phantom.
   2. If any air bubbles are present between the layers, push them out by stroking the surface of the two-layered phantom with a fingertip.
   3. Hold the two-layered phantom between two slide glasses to prevent it drying out.

5. Acquisition of the Diffuse Reflectance Spectra

1. **Acquisition of dark spectra**
   Note: The charge-coupled device (CCD) sensor in the spectrometer can estimate light intensity based on an electrical signal generated in response to incident light. However, there is dark noise[37] which is independent of the signals generated by photons but is dependent on the device temperature, even if the sensor does not detect the light. To accurately measure the spectral intensity of light, the dark current signal should be measured as a dark spectrum and then subtracted from the sample spectrum. The dark spectrum is a spectrum taken with the light path blocked.
   1. Position the integrating sphere at an optimal position for the diffuse reflectance measurements (**Figure 1a**).
   2. Turn off the halogen lamp light source. Block the light path to the spectrometer using a port plug or a shielding plate.
   3. Select the **Store dark** command from the file menu to store a dark spectrum.
   4. Select the **Subtract dark spectrum** command from the file menu to subtract the dark spectrum from the measured sample spectrum (see below).

2. **Acquisition of reference spectra**
   Note: The optical properties of the components used in this experiment, such as the light source, light guide, achromatic lens, optical fiber, and spectrometer, have their own wavelength-dependences. Therefore, the spectral intensity of light passed through these optical components should be measured as a reference spectrum. For the measurement of a diffuse reflectance spectrum, the reference spectrum is a spectrum taken with a standard white diffuser illuminated with the light from the light source.
   1. Turn on the halogen lamp light source by pressing the power button. Warm up the lamp for at least 10 min before acquiring a reference spectrum.
   2. Place a standard white diffuser (*e.g.*, Spectralon) at the sample port of the integrating sphere.
   3. Adjust the integration time of the spectrometer by selecting the suitable value from the drop-down list in the spectrometer operating software so that the peak signal intensity is approximately 75% of the spectrometer intensity maximum.
   4. Select the **Store reference** command from the file menu to store a reference spectrum.

3. **Acquisition of sample spectra**
   Note: A spectrum of the diffuse reflectance of the sample is acquired and saved on the hard drive of a personal computer using the same acquisition conditions.
   1. Place the epidermal phantom sandwiched by the two slide glasses at the sample port. Select the **Save** command from the file menu to save a diffuse reflectance spectrum to a file.
   2. Repeat step 5.3.1 for the dermal and two-layered phantoms.

6. Acquisition of the Total Transmittance Spectrum

1. **Acquisition of dark spectra**
   Note: The sensor in the spectrometer can estimate light intensity based on an electrical signal generated in response to incident light. However, there is dark noise which is independent of the signals generated by photons but is dependent on the device temperature, even if the sensor does not detect the light. To accurately measure the spectral intensity of light, the dark current signal should be measured as a dark spectrum and then subtracted from the sample spectrum. The dark spectrum is a spectrum taken with the light path blocked.
   1. Position the integrating sphere at an optimal position for the total transmittance measurements (**Figure 1b**).
   2. Remove the light trap from the port of the integrating sphere and attach a port plug to the port.
   3. Turn off the halogen lamp light source. Block the light path to the integrating sphere using a port plug or shielding plate.

4. Select the **Store dark** command from the file menu to store a dark spectrum.
5. Select the **Subtract dark spectrum** command from the file menu to subtract the dark spectrum from the measured sample spectrum (see below).

2. **Acquisition of reference spectra**
Note: The optical properties of the components used in this experiment, such as the light source, light guide, achromatic lens, optical fiber, and spectrometer, have their own wavelength-dependences. Therefore, the spectral intensity of the light passed through these components should be measured as a reference spectrum. For the measurement of the total transmittance spectrum, the reference spectrum is a spectrum taken when the light from the light source is directly entering the integrating sphere through the sample port.
    1. Turn on the halogen lamp light source by pressing the power button. Warm up the lamp for at least 10 min before acquiring a reference spectrum.
    2. Regulate the integration time of the spectrometer by selecting the suitable value from the drop-down list of integration times in the operating software of the spectrometer so that the greatest light intensity shows a signal that is approximately 75% of the maximum values.
    3. Select the **Store reference** command from the file menu to store a reference spectrum.

3. **Acquisition of sample spectra**
Note: The spectrum of the total transmittance of the sample is acquired and saved on the hard drive of a personal computer using the same acquisition conditions.
    1. Place the epidermal phantom sandwiched by the two slide glasses at the sample port. Select the **Save** command from the file menu to save a total transmittance spectrum to a file.
    2. Repeat step 6.3.1 for the dermal and two-layered phantoms.

7. Estimating the Absorption and Light-scattering Properties

Note: A set of the diffuse reflectance spectrum and the total transmittance spectrum is saved to the hard drive of a personal computer and analyzed offline. An inverse Monte Carlo simulation[8,38,39,40] is then performed to estimate the absorption coefficient spectrum $\mu_a(\lambda)$ and the reduced scattering coefficient spectrum $\mu_s'(\lambda)$. In this inverse Monte Carlo simulation, the estimated scattering coefficient μ_s, under the assumption that the anisotropy factor g is 0, is regarded as the reduced scattering coefficient μ_s'. Both the reflectance and the transmittance data are used for a single simulation run. The detailed algorithm used in this protocol has been reported in previous literature[8,39]. We estimated the absorption coefficient spectrum $\mu_a(\lambda)$ and the reduced scattering coefficient spectrum $\mu_s'(\lambda)$ of an epidermal layer from a set of the diffuse reflectance spectrum and the total transmittance spectrum obtained from the epidermal layer. In the same way, we estimated $\mu_a(\lambda)$ and $\mu_s'(\lambda)$ of a dermal layer from a set of the diffuse reflectance spectrum and the total transmittance spectrum obtained from the dermal layer.

1. Open an input file for the Monte Carlo simulation.
2. Fill in the values of the measured diffuse reflectance and the total transmittance at the specific wavelength range from 400 to 700 nm at 10 nm-intervals in the input data file. Fill in the value of the phantom thickness in the input data file.
3. Set the refractive index n of a layer to be an appropriate value in the input data file (*e.g.*, n = 1.33 at 550 nm). Set the value of the anisotropy factor g to be 0 in the input data file.
4. Set the initial values of the absorption coefficient μ_a and the scattering coefficient μ_s to be the appropriate values in the input data file (*e.g.*, μ_a = 0.01, μ_s = 0.1).
5. Execute the inverse Monte Carlo simulation program.
6. Type the input file name and then run the simulation.
7. Open the output file and check the final values of μ_a and μ_s after the iterative simulation is terminated.
8. Repeat steps 7.1 - 7.7 for other desired wavelengths.

Representative Results

Figure 3 shows the representative estimated spectra of the reduced scattering coefficient and the absorption coefficient for the epidermal phantom and dermal phantom. The results shown in **Figure 3** are the averages of ten measurements of both reflectance and transmittance spectra. The reduced scattering coefficient μ_s' has a broad scattering spectrum, exhibiting a higher magnitude at shorter wavelengths. The spectral features correspond to the typical scattering spectra of soft tissues. The absorption coefficient μ_a of the epidermal phantom decays exponentially as the wavelength increases, which is similar to the absorption spectrum of melanin. The absorption coefficient spectrum of the epidermal phantom layer and that of melanin[41] were fitted by an exponential function as:

$$\mu_a = A_o + A \cdot e^{(-B\lambda)}$$

The value of B for the epidermal layer was calculated to be 0.011, whereas that for melanin was estimated to be 0.009. The wavelength dependence of the absorption coefficients μ_a for the dermal phantom containing oxygenated blood and deoxygenated blood is dominated by the spectral characteristics of oxygenated hemoglobin and deoxygenated hemoglobin, respectively.

Figure 4 shows representative digital color photographs of the two-layered skin phantoms. **Figure 4a** shows a cross-sectional image of the two-layered skin phantom. **Figure 4b** and **4c** show top views of the 3-by-3 phantom matrix containing oxygenated blood and deoxygenated blood, respectively. The rows from top to bottom have coffee solution concentrations C_c of 5%, 10%, and 20%. The columns from left to right have blood concentrations C_b of 0.2%, 0.4%, and 0.6%. The color of the phantom becomes darker as the value of C_c in the epidermal layer increases, whereas it turns pink as the value of C_b increases. The phantom with oxygenated blood has a more reddish color than that with deoxygenated blood. Those variations represent the change in skin color due to physiological conditions such as tanning and hypoxemia, respectively.

Figure 5 shows an example of representative measured diffuse reflectance spectra obtained from the two-layered skin tissue phantoms having different conditions for (**Figure 5a**) the concentration of coffee solution C_c, (**Figure 5b**) the concentration of whole blood C_b, and (**Figure 5c**) the oxygenated state of blood. In **Figure 5a**, the diffuse reflectance in a shorter wavelength region is significantly decreased in comparison with that in a longer wavelength region as the value of C_c becomes larger. This is due to the strong light absorption by the coffee solution in the shorter wavelength region (see **Figure 3b**). **Figure 5b** shows the remarkable change in diffuse reflectance in the middle wavelength region with the value of C_b, which represents the strong light absorption by hemoglobin in the wavelength range from 500 to 600 nm. The difference in spectral feature between oxygenated hemoglobin and deoxygenated hemoglobin and isosbestic points of hemoglobin are clearly observed in the diffuse reflectance spectra shown in **Figure 5c**.

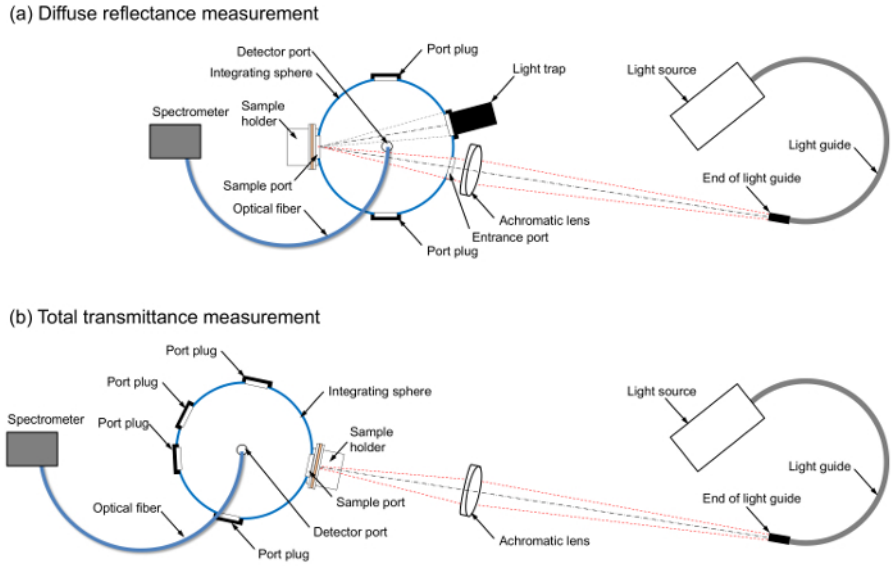

Figure 1: Schematic diagram of the experimental apparatus. These panels show the set-up for measuring (**a**) diffuse reflectance spectra and (**b**) total transmittance spectra. Please click here to view a larger version of this figure.

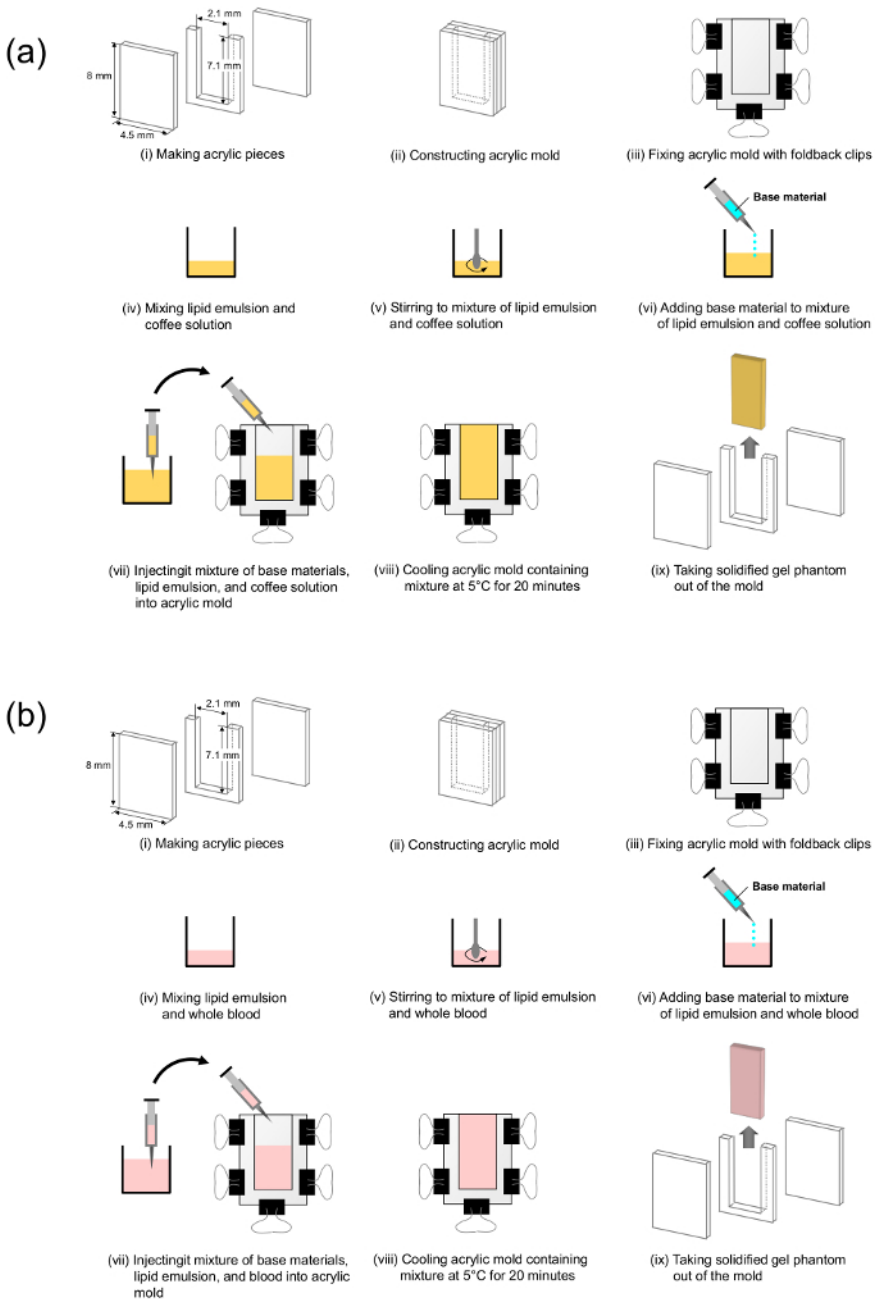

Figure 2: Steps in the preparation of agarose-based optical phantoms. These panels show (**a**) the making of an epidermal layer phantom and (**b**) the making of a dermal layer phantom. Please click here to view a larger version of this figure.

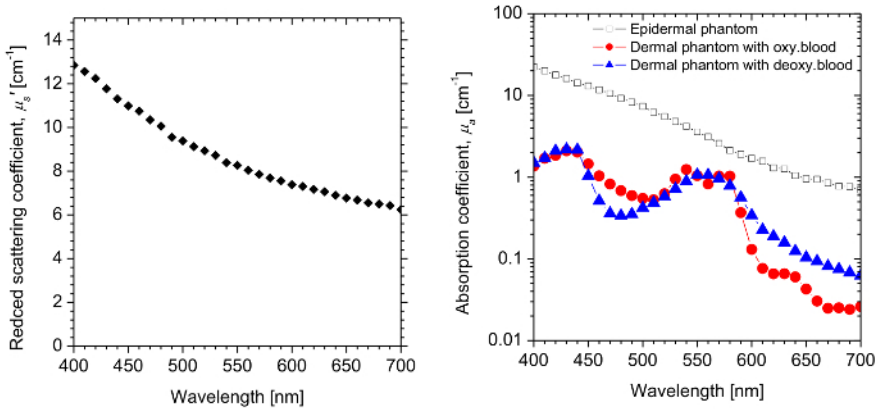

Figure 3: The representative estimated optical properties of phantoms. (**a**) This panel shows the average reduced scattering coefficient spectrum $\mu_s'(\lambda)$ of the epidermal and dermal layers. (**b**) This panel shows the absorption coefficient spectra $\mu_a(\lambda)$ of the epidermal layer and dermal layers. Please click here to view a larger version of this figure.

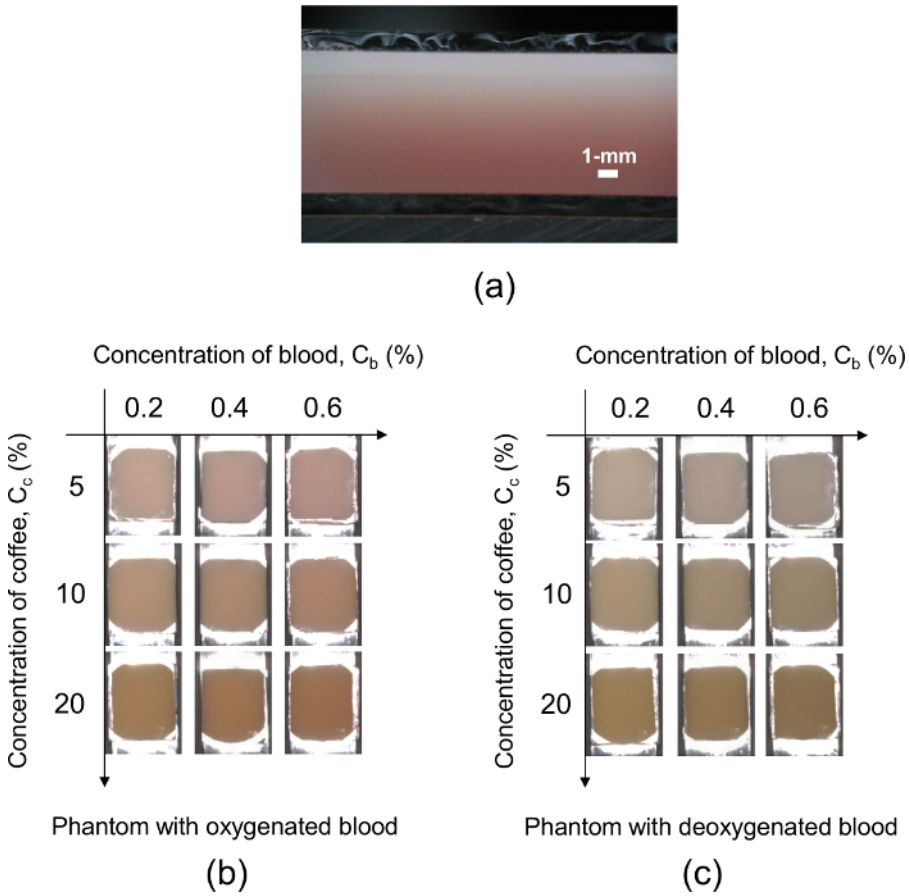

Figure 4: The representative digital color photographs of the two-layered skin phantoms. (**a**) This panel shows a cross-sectional view of the two-layered skin phantom. (**b**) This panel shows the top view of the 3-by-3 phantom matrix containing oxygenated blood. (**c**) This panel shows the top view of the 3-by-3 phantom matrix containing deoxygenated blood. The rows from top to bottom have coffee solution concentrations C_c of 5%, 10%, and 20%. The columns from left to right have blood concentrations C_b of 0.2%, 0.4%, and 0.6%. Please click here to view a larger version of this figure.

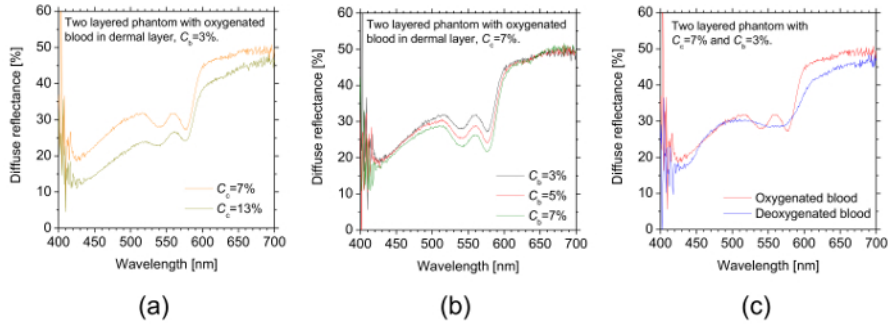

Figure 5: The representative measured diffuse reflectance spectra obtained from the two-layered skin tissue phantoms. These panels show the diffuse reflectance spectra of the phantoms with different conditions of (**a**) the concentration of coffee solution C_c, (**b**) the concentration of whole oxygenated blood C_b, and (**c**) the oxygenated state of blood. Please click here to view a larger version of this figure.

Discussion

The most critical step in this protocol is the temperature control of the base material. The temperature to maintain the base material ranged from 58 to 60 °C. If the temperature is more than 70 °C, a denaturation of both the lipid emulsion and the whole blood will occur. As a consequence, the optical properties of the phantom will deteriorate. If the temperature is less than 40 °C, the base material will be ununiformly gelled and, thus, the light scattering and absorption agents will be heterogeneously distributed in the phantom. Although the base material is kept at 60 °C, suctioning it with a syringe lowers the temperature. The temperature of the base material lowers to 50 °C when it is added to the blood solution.

The optical phantoms described in this article suffer from short useable lifetimes which are usually limited to no more than one day. The useable lifetimes might be extended by encapsulating the phantom with the base material in the sealed container or by using a preservative. The 1-mm-thick epidermal layer phantom is an order of magnitude greater than the human epidermal thickness. In this protocol with the acrylic mold, however, it was difficult to create a layer thickness less than 0.5 mm. To reduce the expected effects of this thickness on the measured diffuse reflectance spectra of the phantoms, the scattering and absorption coefficients of the epidermis phantom were regulated so that the diffuse reflectance spectrum showed the similar spectrum to that of human skin. A spin-coating method[42] looks promising for making a layer thinner than 0.5 mm. The values of μ_a (λ) and μ_s' (λ) for human skin are reported in the literature[43].

The uniform distribution of melanin or bilirubin in an agar phantom layer might be difficult using the protocol described here because those chromophores are not completely soluble in water. The use of melanoidin extracted from roasted coffee beans and tartrazine can be used as comparable or substitute materials for melanin and bilirubin, respectively. The inverse Monte Carlo simulation used for estimating the optical properties from the measured diffuse reflectance and the total transmittance is relatively time-consuming due to its iterative fashion. Another light transport calculation model such as the adding-doubling method[44] can be used to shorten the calculation time. The reduced scattering coefficient μ_s' is a lumped optical property incorporating the scattering coefficient μ_s and the anisotropy factor g. To estimate μ_s and g separately, the collimated transmittance of a phantom must be measured in addition to the total transmittance and the diffuse reflectance[38,40]. In the present study, we did not measure the refractive index for each layer. We set the refractive index of water as published in literature[45] in the input data file for the inverse Monte Carlo simulation instead since the agarose gel consists mainly of water. We assumed that there is no difference in the refractive indices between the two layers. We also used the nominal value for the refractive index of glass (*e.g.*, n = 1.524 at λ = 546.1 nm) for the Monte Carlo simulations.

It is advantageous that this protocol, with one integrating sphere instead of two integrating spheres, is cost-effective. On the other hand, using a single integrating sphere is time-consuming since the arrangement of the integrating sphere must be changed according to whether the measurement is for a total transmittance or for a diffuse reflectance. It is advantageous that the protocol described in this article can extend to create monolayer or multilayer optical phantoms with various shapes, sizes, and inclusions by changing the design of the molds. The surfaces of the phantom layers were wetted immediately after they were taken out of their mold. Therefore, the epidermal layer and dermal layer were adhered together by stacking the second layer closely onto the first layer. It might be possible to solidify the second layer directly on the first one, rather than fabricating them separately and attaching them afterward. In that case, however, it may be difficult to accurately make a thin epidermal layer with a uniform layer thickness. We sandwiched the phantom between the glasses to prevent a drying of the phantom. We considered the optical properties and thickness of glass in the inverse Monte Carlo simulation. Therefore, there is no effect on the estimated optical properties of the phantoms. The significance of the present technique with respect to existing methods is its ability to represent the diffuse reflectance spectra of living tissues in the visible to near-infrared wavelength region. The optical phantoms made by this protocol will be available for validation of newly developed optical methods based on diffuse reflectance spectroscopy and spectrocolorimetry.

Disclosures

The authors have nothing to disclose.

Acknowledgements

Part of this work was supported by a Grant-in-Aid for Scientific Research (C) from the Japanese Society for the Promotion of Science (25350520, 22500401, 15K06105) and the US-ARMY ITC-PAC Research and Development Project (FA5209-15-P-0175, FA5209-16-P-0132).

References

1. Pogue, B. W., Patterson, M. S. Review of tissue simulating phantoms for optical spectroscopy, imaging and dosimetry. *Journal of Biomedical Optics.* **11** (4), 041102 (2006).
2. Cohen, G. Contrast--detail--dose analysis of six different computed tomographic scanners. *Journal of Computer Assisted Tomography.* **3** (2), 197-203 (1979).
3. Seltzer, S. E., Swensson, R. G., Judy, P. F., Nawfel, R. D. Size discrimination in computed tomographic images. Effects of feature contrast and display window. *Investigative Radiology.* **23** (6), 455-462 (1988).
4. Pifferi, A. *et al.* Performance assessment of photon migration instruments: the MEDPHOT protocol. *Applied Optics.* **44** (11), 2104-2114 (2005).
5. Prahl, S. A. *Project: Optical Phantoms.* http://omlc.org/~prahl/projects/phantoms.html. (2014).
6. Linford, J., Shalev, S., Bews, J., Brown, R., Schipper, H. Development of a tissue-equivalent phantom for diaphanography. *Medical Physics.* **13** (6), 869-875 (1986).
7. Durkin, A. J., Jaikumar, S., Richardskortum, R. Optically dilute, absorbing, and turbid phantoms for fluorescence spectroscopy of homogeneous and inhomogeneous samples. *Applied Spectroscopy.* **47** (12), 2114-2121 (1993).
8. Nishidate, I., Aizu, Y., Mishina, H. Estimation of melanin and hemoglobin in skin tissue using multiple regression analysis aided by Monte Carlo simulation. *Journal of Biomedical Optics.* **9** (4), 700-710 (2004).
9. Nishidate, I., Maeda, T., Aizu, Y., Niizeki, K. Visualizing depth and thickness of a local blood region in skin tissue using diffuse reflectance images. *Journal of Biomedical Optics.* **12** (5), 054006 (2007).
10. Nishidate, I. *et al.* Noninvasive imaging of human skin hemodynamics using a digital red-green-blue camera. *Journal of Biomedical Optics.* **16** (8), 086012 (2011).
11. Bharathiraja, S. *et al.* Multimodality tissue-mimicking phantom for thermal therapy. *Physics in Medicine & Biology.* **49** (13), 2767-2778 (2004).
12. Firbank, M., Oda, M., Delpy, D. T. An improved design for a stable and reproducible phantom material for use in near-infrared spectroscopy and imaging. *Physics in Medicine & Biology.* **40** (5), 955-961 (1995).
13. Hebden, J. C., Hall, D. J., Firbank, M., Delpy, D. T. Timeresolved optical imaging of a solid tissue-equivalent phantom. *Applied Optics.* **34** (34), 8038-8047 (1995).
14. Firbank, M., Delpy, D. T. A phantom for the testing and calibration of near-infrared spectrometers. *Physics in Medicine & Biology.* **39** (9), 1509-1513 (1994).
15. Sukowski, U., Schubert, F., Grosenick, D., Rinneberg, H. Preparation of solid phantoms with defined scattering and absorption properties for optical tomography. *Physics in Medicine & Biology.* **41**, 1823-1844 (1996).
16. Vernon, M. L., Freàchette, J., Painchaud, Y., Caron. S., Beaudry, P. Fabrication and characterization of a solid polyurethane phantom for optical imaging through scattering media. *Applied Optics.* **38** (19), 4247-4251 (1999).
17. Lualdi, M., Colombo, A., Farina, B., Tomatis, S., Marchesini, R. A phantom with tissue-like optical properties in the visible and near infrared for use in photomedicine. *Lasers in Surgery and Medicine.* **28** (3), 237-243 (2001).
18. Dabbagh, A., Abdullah, B. J., Ramasindarum, C., Abu Kasim, N. H. Tissue-mimicking gel phantoms for thermal therapy studies. *Ultrasonic Imaging.* **36** (4), 291-316 (2014).
19. Cabrelli, L. C., Pelissari, P. I., Deana, A. M., Carneiro, A. A., Pavan, T. Z. Stable phantom materials for ultrasound and optical imaging. *Physics in Medicine & Biology.* **62** (2), 432-447 (2017).
20. Vogt, W. C., Jia, C., Wear, K. A., Garra, B. S., Pfefer, T. J. Biologically relevant photoacoustic imaging phantoms with tunable optical and acoustic properties. *Journal of Biomedical Optics.* **21** (10), 101405 (2016).
21. Bays, R. *et al.* Three-dimensional optical phantom and its application in photodynamic therapy. *Lasers in Surgery and Medicine.* **21** (3), 227-234 (1997).
22. Ramella-Roman, J. C., Bargo, P. R., Prahl, S. A., Jacques, S. L. Evaluation of spherical particle sizes with an asymmetric illumination microscope. *IEEE Journal of Selected Topics in Quantum Electronics.* **9** (2), 301-306 (2003).
23. Waterworth, M. D., Tarte, B. J., Joblin, A. J., van Doorn, T., Niesler, H. E. Optical transmission properties of homogenised milk used as a phantom material in visible wavelength imaging. *Australasian Physical and Engineering Science in Medicine.* **18** (1), 39-44 (1995).
24. Moes, C. J, van Gemert, M. J., Star, W. M., Marijnissen, J. P., Prahl, S. A. Measurements and calculations of the energy fluence rate in a scattering and absorbing phantom at 633 nm. *Applied Optics.* **28** (12), 2292-2296 (1989).
25. van Staveren, H. J, Moes, C. J., van Marie, J., Prahl, S. A., van Gemert, M. J. Light scattering in intralipid-10% in the wavelength range of 400-1100 nm. *Applied Optics.* **30** (31), 4507-4514 (1991).
26. Flock, S. T., Jacques, S. L., Wilson, B. C., Star, W. M., Vangemert, M. J. C. Optical-properties of intralipid - a phantom medium for light-propagation studies. *Lasers in Surgery and Medicine.* **12** (5), 510-519 (1992).
27. Madsen, S. J., Patterson, M. S., Wilson, B. C. The use of India ink as an optical absorber in tissue-simulating phantoms. *Physics in Medicine & Biology.* **37**, 985-993 (1992).
28. Cubeddu, R., Pifferi, A., Taroni, P., Torricelli, A., Valentini, G. A solid tissue phantom for photon migration studies. *Physics in Medicine & Biology.* **42** (10), 1971-1979 (1997).
29. Ebert, B. *et al.* Near-infrared fluorescent dyes for enhanced contrast in optical mammography: phantom experiments. *Journal of Biomedical Optics.* **6** (2), 134-140 (2001).
30. Sukowski, U., Schubert, F., Grosenick, D., Rinneberg, H. Preparation of solid phantoms with defined scattering and absorption properties for optical tomography. *Physics in Medicine & Biology.* **41**, 1823-1844 (1996).
31. Yoshida, K., Nishidate, I., Ishizuka, T., Kawauchi, S., Sato, S, Sato, M. Multispectral imaging of absorption and scattering properties of *in vivo* exposed rat brain using a digital red-green-blue camera. *Journal of Biomedical Optics.* **20** (5), 051026 (2015).
32. Lo, J. Y. *et al.* A strategy for quantitative spectral imaging of tissue absorption and scattering using light emitting diodes and photodiodes. *Optics Express.* **17** (3), 1372-1384 (2009).
33. Bednov, A., Ulyanov, S., Cheung, C., Yodh, A. G. Correlation properties of multiple scattered light: implication to coherent diagnostics of burned skin. *Journal of Biomedical Optics.* **9** (2), 347-352 (2004).

34. Hull, E. L., Nichols, M. G., Foster, T. H. Quantitative broadband near-infrared spectroscopy of tissue-simulating phantoms containing erythrocytes. *Physics in Medicine & Biology.* **43** (11), 3381-3404 (1998).
35. Kienle, A., Patterson, M. S., Ott, L., Steiner, R. Determination of the scattering coefficient and the anisotropy factor from laser Doppler spectra of liquids including blood. *Applied Optics.* **35** (19), 3404-3412 (1996).
36. Srinivasan, S., Pogue, B. W., Jiang, S., Dehghani, H., Paulsen, K. D. Spectrally constrained chromophore and scattering NIR tomography improves quantification and robustness of reconstruction. *Applied Optics.* **44** (10), 1858-1869 (2004).
37. Ocean Optics Inc. *Glossary. Dark Noise.* https://oceanoptics.com/glossary/#d (2018).
38. Friebel, M., Roggan, A., Müller, G., Meinke, M. Determination of optical properties of human blood in the spectral range 250 to 1100 nm using Monte Carlo simulations with hematocrit-dependent effective scattering phase functions. *Journal of Biomedical Optics.* **11** (3), 34021 (2006).
39. Nishidate, I., Aizu, Y., Mishina, H. Estimation of absorbing components in a local layer embedded in the turbid media on the basis of visible to near- infrared (VIS-NIR) reflectance spectra. *Optical Review.* **10** (5) 427-435 (2003).
40. Friebel, M., Helfmann, J., Netz, U., Meinke, M. Influence of oxygen saturation on the optical scattering properties of human red blood cells in the spectral range 250 to 2000 nm. *Journal of Biomedical Optics.* **14** (3), 034001 (2009).
41. Jacques, S. L., Glickman, R. D., Schwartz, J. A. Internal absorption coefficient and threshold for pulsed laser disruption of melanosomes isolated from retinal pigment epithelium. *SPIE Conference Proceedings.* **2681**, 468-477 (1996).
42. Park, J., Ha, M., Yu, M., Jung B. Fabrication of various optical tissue phantoms by the spin-coating method. *Journal of Biomedical Optics.* **21** (6), 065008 (2016).
43. Jacques S. L. *Skin Optics.* https://omlc.org/news/jan98/skinoptics.html. (1998).
44. Prahl, S. A., van Gemert, M. J. C., Welch, A. J. Determining the optical properties of turbid media by using the adding-doubling method. *Applied Optics.* **32** (4) 559-568 (1993).
45. Hale, G. M., Querry, M. R. Optical constants of water in the 200-nm to 200-um wavelength region. *Applied Optics.* **12** (3), 555-563 (1973).

